Fire behaviour of EPDM/NBR panels with paraffin for thermal energy storage applications. Part 2: Analysis of the combustion residues

Francesco Valentini, Emanuela Callone, Sandra Dirè, Jean-Claude Roux, J. Lopez-Cuesta, Gwenn Le Saout, Luca Fambri, Andrea Dorigato, Alessandro Pegoretti

Fire behaviour of EPDM/NBR panels with paraffin for thermal energy storage applications. Part 2: Analysis of the combustion residues

Francesco Valentini [a,*], Emanuela Callone [b], Sandra Dirè [b], Jean-Claude Roux [c], Josè-Marie Lopez-Cuesta [c,*], Gwenn le-Saout [c], Luca Fambri [a], Andrea Dorigato [a], Alessandro Pegoretti [a,*]

[a] University of Trento, Department of Industrial Engineering and INSTM Research Unit, via Sommarive 9, 38123 Trento, Italy
[b] "Klaus Müller" NMR Laboratory, University of Trento, via Sommarive 9, 38123 Trento, Italy
[c] Polymer Composites Hybrids (PCH) – IMT Mines Alès, 6 avenue de Clavières, 30319 Alès Cedex, France

A B S T R A C T

In the first part of this work, novel elastomeric panels with paraffin for thermal energy storage applications were developed. Ethylene-Propylene Diene Monomer (EPDM) rubber filled with a shape-stabilized paraffin, as phase change material with a melting temperature of 28 °C, was covered with a nitrile-butadiene rubber (NBR) en-velope. In order to improve the fire resistance, two selected flame retardants (FRs) were dispersed both in the EPDM core and in the NBR envelope. In this work, the combustion residues from cone calorimeter tests were analysed by various techniques to explain the combustion mechanisms and the interaction of FRs. Nuclear magnetic resonance (NMR) evidenced the complexity of the system, characterized by the formation of char, by the reactivity of organomodified montmorillonite (oMMT) in presence of phosphates and structural rearrange-ments of the inorganic components. The use of a flame retardant based on ammonium polyphosphate and synergistic agents (based on phosphorus) led to formation of different Al-O-P and Si-O-P compounds. The X-ray diffraction (XRD) analysis highlighted that the formation of silicon phosphate, from the reaction of ammonium polyphosphate and oMMT, was possible only at high phosphorus contents. From the phosphorus content detected through energy dispersive X-ray spectroscopy (EDX) it was possible to indicate that the phosphorus remained in the condensed phase during the combustion.

Keywords:
Flame retardancy
Rubber panels
Phase change materials
X-ray diffraction
Nuclear magnetic resonance

1. Introduction

Energy is a key pillar for human well-living. In recent years, due to the rapid demographic growth and the boosting of the industrial production, energy consumption became a burden on conventional energy resources, due to the continuous increase of climate altering emissions and the consequences in terms of climate change [1,2]. It is therefore essential to find an equilibrium between energy demand and energy resources [3]. The need for the reduction of CO_2 emissions and the increasing awareness of the limits of non-renewable energy resources has stimulated the demand of renewable energy sources, like the solar power [4,5]. Considering the fact that the residential sector, in 2018, contributed for 17% of the total CO_2 emissions in the EU and that around 78% of this contribution was due to space heating and domestic hot water, thermal energy storage (TES) seems to be a promising and critical technology for the next years [6,7]. Thermal energy storage is a technology based on the phase transition from the solid to the liquid state (and vice-versa) of particular materials, called Phase Change Materials (PCMs), that occurs at constant temperature and provides high energy storage capability [8–13]. Paraffins are the most used PCMs thanks to the high heat of fusion, low price, chemical stability and wide range of melting temperature [9-11,14]. Possible application of paraffinic PCMs are for the thermal energy storage of buildings: examples are the integration of paraffinic PCMs with heat pumps [15] or with solar water heating systems [16–18], wallboards made of expanded perlite containing paraffin [19], wallboards made of expanded graphite containing paraffin [20], wallboards made of cellulose containing paraffin [21], gypsum boards containing paraffin [22], concrete containing paraffin

* Corresponding authors.
E-mail addresses: francesco.valentini@unitn.it (F. Valentini), jose-marie.lopez-cuesta@mines-ales.fr (J.-M. Lopez-Cuesta), alessandro.pegoretti@unitn.it (A. Pegoretti).

for floor or wall applications, rubber panels containing paraffin such as EPDM/NBR panels [23].

The main safety problem in using paraffinic PCMs in building application is their flammability and the fact that in case of fire they represent an additional fuel source. In the literature different methods to reduce the flammability have been reported: one possibility is the encapsulation of the composite building block within two layers of non-combustible concrete, a second one consists in the combined use of a shape-stabilizer for the PCM (a polymeric matrix) and flame retardants (FRs) [24,25]. One of the most interesting classes of flame retardants is represented by the intumescent-materials, which consist of a precursor of carbonization catalyst such as ammonium polyphosphate (APP), a carbonization agent such as pentaerythritol (PER) and a blowing agent such as melamine polyphosphate (MPP). The working principle is the formation, when heated beyond a critical temperature, of an intumescent layer thanks to the combination of a charring and foaming mechanism. This layer is able to protect the underlying material from excessive temperature increase, oxygen diffusion and exposure to the ignition source [26–30]. The performances of flame retardants can be improved by using synergistic agents, such as for example oMMT and talc with APP. The effect of montmorillonite combined with intumescent flame retardants has been widely reported and consists in the formation of a carbonaceous-silicate charred layer that preserves the underlying material from excessive temperature increase [31–33]. Similarly, the use of talc leads to the formation of a protective silicate layer for the underlying material [34,35]. Also the use of kaolin leads to a synergism when combined with intumescent flame retardants (APP + pentaerythritol + melamine), as it was verified by Thuechart et al. [36]. Considering the possible application of EPDM/NBR paraffin panels for building applications, characterized in our previous work [23], and the risks associated to the use of such materials in case of fire, the fire behaviour of these rubber panels was deeply studied, and the effects of four different flame retardants were compared and reported in the Part 1 of the research [37]. In order to shed more light on the combustion mechanisms, the best two compositions were selected for further investigations, as Part 2 of the research.

This article focuses on the characterization of the combustion residues, on the interactions between the fillers present in the core material and in the envelope material with APP and between the components present in the flame retardant with APP: multinuclear solid state nuclear magnetic resonance (ssNMR), X-Ray Diffraction (XRD), Scanning Electron Microscopy (SEM) and Energy Dispersive X-Ray Spectroscopy (EDX) were used as investigation techniques.

2. Experimental part

2.1. Materials

Vistalon® 2504 EPDM rubber was purchased from Exxon Mobil (Irving, TX, USA). It is characterized a low Mooney viscosity (ML 1 + 4, 125 °C) of 25 MU, a medium diene content (4.7 wt% of ethylidene norbornene), a low ethylene content (58 wt%) and it shows an excellent resistance to UV and ozone due to the saturated polymer backbone [38]. Rubitherm RT28HC paraffinic wax, with a melting temperature of 28 °C, was purchased from Rubitherm GmbH (Berlin, Germany). Carbon black N550 obtained from Omsk Carbon group (Omsk, Russia) was used as a reinforcing filler. Zinc oxide (curing activator), stearic acid (curing activator and lubricating agent) and sulphur (vulcanizing agent) were supplied by Rhein Chemie (Cologne, Germany). The accelerators tetramethylthiuram disulphide (TMTD) and zinc dibutyl dithiocarbamate (ZDBC) were obtained from Vibiplast srl (Castano Primo (MI), Italy). The elastomeric compound used for the preparation of the samples consisted of: Vistalon® 2504 (100 phr), sulphur (3 phr), zinc oxide (3 phr), stearic acid (1 phr), carbon black (20 phr), TMTD (0.87 phr) and ZDBC (2.5 phr).

Organomodified montmorillonite (oMMT) Cloisite® 20 was obtained from BYK-Chemie GmbH (Wesel, Germany). Cloisite®20 is a bentonite (or montmorillonite) modified with bis(hydrogenated tallow alkyl) dimethyl ammonium chloride. It has a density of 1.8 g/cm^3, a particle size lower than 10 μm and by a lamellar spacing of 3.2 nm [39–41].

Exolit® AP766 (766), a non-halogenated FR based on the synergism between phosphorus and nitrogen, was provided by Clariant GmbH (Ahrensburg, Germany). As reported in the supplementary materials (section S1.2), this FR contained APP, aluminium diethyl phosphinate and probably MPP. Exolit® AP423 (423), a non-halogenated FR consisting of APP (phosphorus content around 31 wt%), was provided by Clariant GmbH (Ahrensburg, Germany).

NBR (nitrile-butadiene rubber) foils (thickness of 0.4 mm), with 45 wt% of acrylonitrile content, without FR (used as reference) and with 18 wt% of FR were purchased on the market. The neat NBR compounds contained around 33 wt% of inorganic fillers in their composition (i.e. talc (11 wt%), kaolin (11 wt%) and silica (11 wt%)). Talc Mistron® R10 C was provided by Imerys Talc (Paris, France). Kaolin ARGIREC™ B24 was provided by Imerys Talc (Paris, France). Silica ULTRASIL VN 3 was provided by Evonik AG (Essen, Germany).

All the above-mentioned ingredients were commercial grade, no specific purity was used.

2.2. Sample preparation

In this work the combustion residues of three selected samples tested through cone calorimeter in Part 1 [37] have been studied. For the detailed description of the preparation of composites the reader is invited to refer to the previous paper.

Samples for cone calorimeter test consisted of an EPDM matrix containing paraffin premixed with oMMT, and by an external envelope made of NBR rubber used to avoid paraffin leakage.

Samples were prepared by melt compounding in an internal mixer (Thermo Haake Rheomix® 600), at 40 °C and a rotating speed of 50 rpm. First, the EPDM sample was prepared according to the composition previously reported: the elastomer was fed into the mixer with the carbon black and mixed for 5 min, then sulphur, zinc oxide, stearic acid and the accelerators were added and mixed for other 5 min. The PCM-clay mixture was then added to the mixer and mixed for 30 min, followed by the FR that was gradually added and mixed for further 10 min, reaching a total mixing time of 50 min. The compounds were then covered with a NBR envelope (thickness 0.4 mm), placed into a mould, and vulcanized under a Carver hot press at a pressure of 2 bar, for 20 min at a temperature of 170 °C. In this way, square sheets with dimensions of around 110×110×5 mm^3 were obtained.

The prepared samples were then burnt during the cone calorimeter tests and the residual material was recovered to be further analysed. As it is possible to observe from Fig. 1, after the combustion it was still possible to clearly identify the material forming the core and the envelope. The two residues were therefore separated and analysed.

The list of the tested samples along with their codes is reported in Table 1. It should be highlighted that each sample, after combustion, was divided into two sub-samples: the Core material and the Envelope.

2.3. Experimental methodologies

Solid-state NMR analyses were performed with a 9.4 T Bruker Avance 400WB spectrometer equipped with a double resonance CPMAS probe under Magic Angle Spinning (MAS) using single pulse sequence. Typical experimental parameters were: ^{13}C) frequency of 100.48 MHz, π/2 flip angle of 4.4 μs, recycle delay of 3 s and 10k transients; ^{31}P) frequency of 161.97 MHz, π/4 flip angle of 3.9 μs, recycle delay of 120 s and 128 transients; ^{27}Al) frequency of 104.26 MHz, π/12 flip angle of 2 μs, recycle delay of 1 s and 1k transients; ^{29}Si) frequency of 79.57 MHz, π/4 flip angle of 2.2 μs, recycle delay of 100 s and 2k transients. Samples were packed in 4 mm zirconia rotors, which were spun at 12 kHz under air flow. Adamantane, Octakis(trimethylsiloxy)silsesquioxane (Q8M8),

Fig. 1. Picture of the combustion residues after cone calorimeter of Sample 1 ($E + P +$ ENV). It should be noticed that the top layer of the combustion residues of the envelope has been manually removed in order to make visible the combustion residues of the core material. The bottom layer of the combustion residues of the envelope is still visible.

$Al(NO_3)_3$ 1 M and diphosphatidic acid (ADP) were used as external secondary references. Usual notation for silicates and phosphates in ^{29}Si and ^{31}P NMR are used: Q^n stands for $Si(OSi)_n(OX)^{4-n}$, Q'^n stands for $OP(OP)_n(OX)^{3-n}$. Profile fitting analyses were performed assuming Gaussian/Lorenzian lineshapes for half integer spin nuclei and Czjzek model [42] for quadrupolars with Topspin 3.6™ and DMfit™ [43] softwares, with a confidence level of 95%.

X-ray diffraction analyses were performed using a diffractometer BRUKER D8 Advance, with an incident beam angle (radiation wavelength of 0.1540598 nm) varying between 5° and 75° X'Pert High Score Plus™ software (version 2.1) was used to process diffraction patterns.

Energy dispersive X-Ray spectroscopy was performed using a Oxford XmaxN system and a detector with a resolution of 133 eV. Only samples 1 and 2 have been studied using this technique.

Scanning electron microscopy (SEM) was performed using a Quanta FEG 200 (FEI company) scanning electron microscope, operating in high vacuum at an acceleration voltage of 12.5 kV. Only samples 1 and 2 have been studied using this technique.

3. Results and discussion

3.1. Nuclear magnetic resonance (NMR)

Taking in to account the complexity of the sample compositions with possible both amorphous and crystalline combustion residues, the materials were at first analysed through multinuclear solid-state NMR.

Carbon −13 spectra show the residue of the combustion of the organic matrices. The ^{13}C MAS NMR spectrum of the neat core materials, i.e. commercial EPDM is presented in Supplementary materials (see Figure S3). The char spectra of the Samples 1, 2 and 3 (to which also paraffin, oMMT, carbon black and catalyst are added), presented in Fig. 2a, show the almost complete disappearance of the aliphatic signals (60–0 ppm region), especially for Sample 3. The three composites originate a similar carbon spectrum dominated by the very broad resonance centred at 130 ppm, due to the carbon black and the graphitic-like residue of the burnt organic components [44,45].

Similarly, the carbon-13 spectra of the combustion residues of the envelopes of Samples 1, 2 and 3, shown in Fig. 2b, present mainly a broad resonance in the aromatic range together with a small signal in the

Table 1
Code and composition of the prepared samples with and without FRs.

Sample code	FR in Core [wt% - phr]	FR in Env [wt% - phr]	PCM* [wt% - phr]	EPDM content [g]	Total mass Core [g]	Total mass Env [g]	PCM content [g]
Sample 1 ($E + P$+ENV)	0	0	56.8 - 263	10.3	~ 48	~ 16	~ 27
Sample 2 ($E + P +$ 766+ENV+766)	20 - 115	18 - 40	45.5 - 263	8.3	~ 48	~ 16	~ 22
Sample 3 ($E + P +$ 423+ENV+423)	20 - 115	18 - 40	45.5 - 263	8.3	~ 48	~ 16	~ 22

* PCM content evaluated with respect to the total mass of the core material (not considering the envelope).
Acronyms: FR = flame retardant, E = EPDM, P = PCM, ENV=NBR envelope, 766=Exolit® AP766, 423=Exolit® AP423.

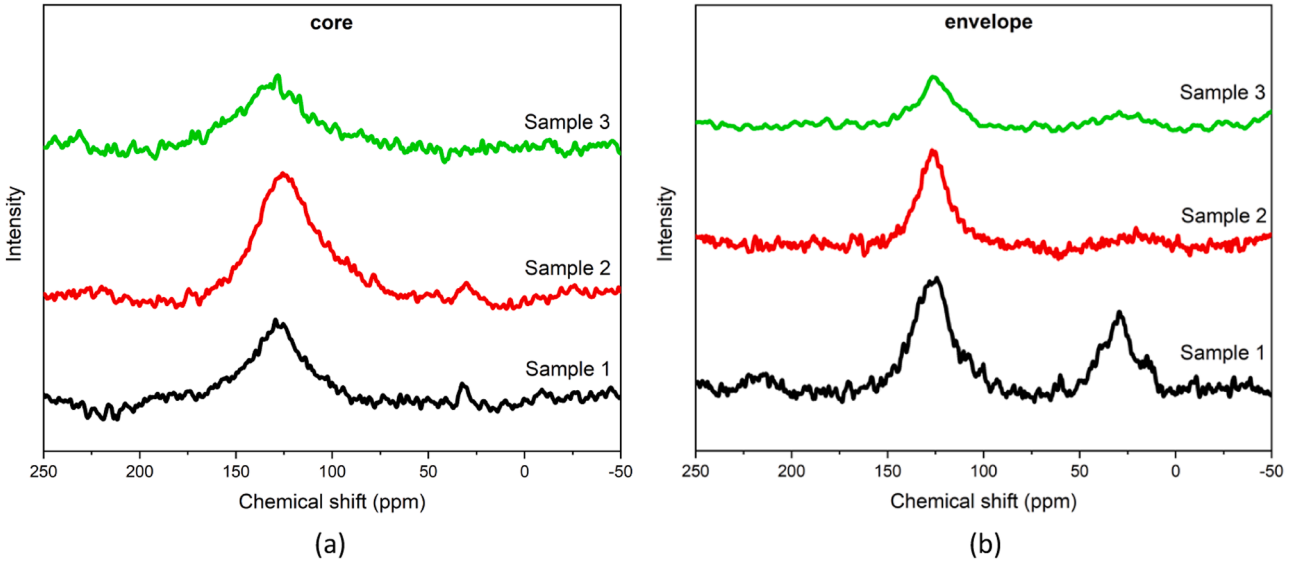

Fig. 2. ^{13}C MAS NMR spectra of the combustion residues of core material (a), ^{13}C CPMAS NMR spectra of envelope (b) of Samples 1, 2, 3.

aliphatic region, as expected comparing these results with the carbon spectrum of the neat envelope (see Figure S3b), which is dominated by the NBR peaks [44,45]. The combustion causes a reduction of the aliphatic C in favour of the graphitic component that broadens, as shown in the spectrum of Sample 1. The addition of phosphorus-based FRs in Samples 2 and 3 strengthens this effect, reducing the aliphatic signal almost to zero and also modifying the lineshape of the char signal. Taking into account the molecular structures of the additives (APP, aluminium diethyl phosphinate), the formation of N-based heterocycles, phenolic species and phosphor-carbonaceous structures in the char seems reasonable [46].

Considering the composition of the intumescent and synergic compounds, aluminium, silicon and phosphorus spectra were also investigated. The presence of oMMT and, only in Sample 2, of aluminium diethyl phosphinate in the core material is visible in the ^{27}Al MAS spectra of Fig. 3a. The spectrum of sample 1 shows the oMMT features with a main resonance centred at about − 5 ppm, due to the octahedral Al sites and a small one at 60 ppm due to some tetrahedral Al units [47,48]. In Samples 2 and 3 the main resonance appears upfield-shifted and two components can be seen: a very broad one at about − 18 ppm overlapped with a relatively sharp one at about − 16 ppm. These components account for 73% and 27%, respectively, in both samples, and represent Al in octahedral sites with phosphorus atoms as second nearest neighbours (Al[OP]$_6$), which are responsible for the large field shift [46,49]. According to these results oMMT in the presence of phosphates reacts to a great extent.

In the envelope composition kaolin replaces oMMT; accordingly, its aluminium-27 spectrum presents one broad peak at about 8 ppm, due to octahedral aluminium in a gibbsite structure (Figure S4, sample 1 neat) [50]. The decomposition, due to cone calorimetry, induces a partial conversion to tetrahedral aluminium as indicated by the very broad resonance from 80 to 50 ppm in Sample 1 (Fig. 3b). When the formulation contains P-based compounds, such as aluminium phosphinates or phosphates, as in Samples 2 and 3, the octahedral kaolin at 8 ppm and a negligible amount of tetrahedral Al at 72 ppm are still present together with two new signals at 45 and − 10 ppm. These can be attributed to AlO_4 and AlO_6 units with vertex oxygens linked to phosphorus [44,49,51]. The tetrahedral Al-O-P is a relatively sharp peak and is clearly present only in Sample 2, suggesting that it derives from the degradation of aluminium diethyl phosphinates present in AP766 (see Figure S4). Moreover, its upfield chemical shift with respect to the usual AlO_4 range could be explained by the bonding with P creating alternate AlO_4 and PO_4 units, indicating a reaction between kaolin and APP [49]. Due to the broadening, especially in Sample 1, a minor amount of AlO_5, frequently found in thermally-treated kaolin, cannot be excluded.

The presence of silicon in the residues of the core materials derives from the presence of oMMT, whose ^{29}Si NMR spectrum ([47]) is composed by a main resonance at −92.5 ppm due to Q^3(0Al) units (i.e. silicon atoms connected to three SiO_4 tetrahedra by basal oxygen atoms, and to the octahedral sheets via apical tri-coordinated oxygen atoms), a shoulder at −87.5 ppm due to Q^3(1Al) units (i.e. silicon atoms linked to one four-fold coordinated Al atom and connected to the octahedral sheet by an apical oxygen atom) [47,48]. Moreover, minor contributions of Q^4 units centred at about −110 ppm and at −111 and −104 ppm due to Q^4(0Al) and Q^4(1Al) units are present [47]. The silicon-29 spectrum of the combustion residue of Sample 1 core material (Fig. 4a) shows two broad peaks at −93.3 and - 110.3 ppm, accounting for the reduction of the main oMMT resonance in favour of the Q^4 (i.e. pure silica) one [47,48]. Moreover, it can be observed that the former peak still decreases in the spectrum of Sample 2, and almost disappears in the spectrum of Sample 3, where only the silica resonance is present together with a peak at −217 ppm, attributable to 6-fold coordinated Si, as in $Si_5O(PO)_6$ (which has one unique P site, and three inequivalent Si sites: one Si(1) 6-fold coordinated, two Si(2) 6-fold coordinated, two Si(3) 4-fold coordinated) [52,53].

In the silicon-29 spectrum of the envelope of Sample 1 before combustion, shown in Figure S5, it is possible to observe five overlapped resonances. The broad resonance centred at −110 ppm with a shoulder at −100 ppm is due to the pure silica Q^4 and Q^3 units [54]. The peak centred at −90.3 ppm can be associated to the silicon sites in kaolin [55]. The signal at −95.2 ppm belongs to talc ($Mg_3Si_4O_{10}(OH)_2$), as two tetrahedral silicate sheets with an octahedral sheets of MgO(OH) in between [56]. The combustion of the envelope of Sample 1 (Fig. 4b) causes a clear broadening of kaolin resonance. Samples 2 and 3 originate similar silicon spectra with different ratios of the above-described components, due to the silicate structural rearrangements caused by the heat; the results of the profile fitting analysis of ^{29}Si MAS NMR spectra are listed in Table 2. In all samples, it is clear that the cone calorimetry significantly impacts on the structure of kaolin, and talc, whose resonances reduce in favour of the amorphous silica network with a small amount of intercalated tetrahedral Al.

Finally the phosphorus-31 (^{31}P MAS) spectra were recorded for Sample 2 and 3 (both cores and envelopes) to study the reaction undergone by the selected intumescent compounds. The cores give rise in Fig. 5a to overlapped broad resonances. Two broad resonances in the regions 0–20 ppm and −20/−80 ppm are visible, the latter being

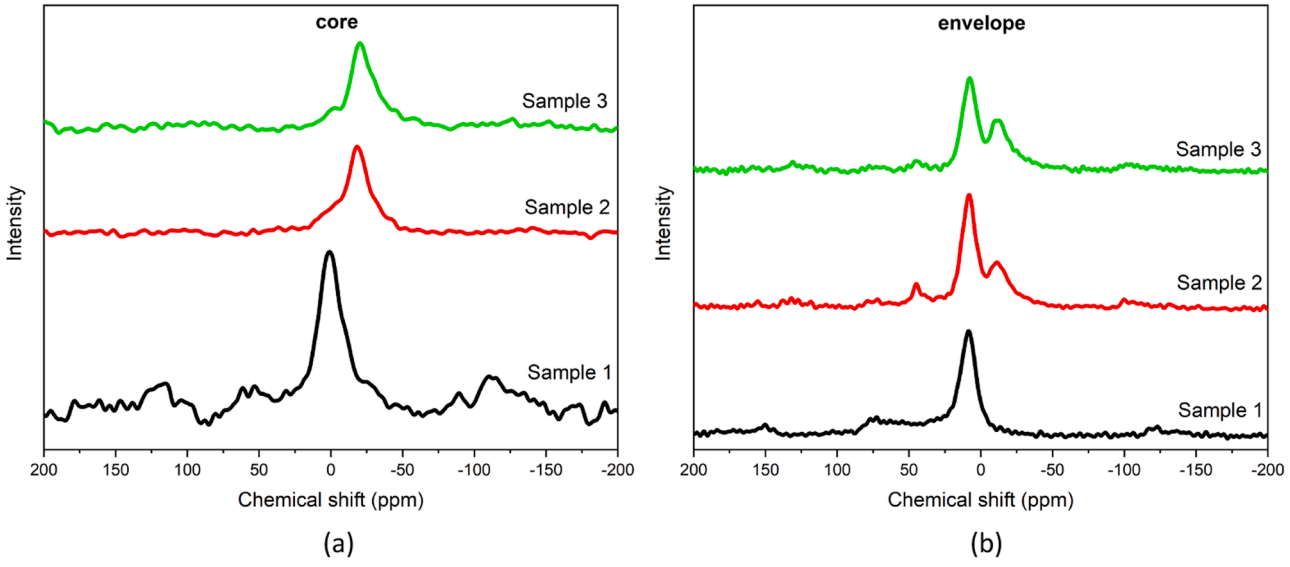

Fig. 3. ^{27}Al MAS NMR spectra of the combustion residues of the core material (a) and of envelope (b) of Samples 1, 2, 3.

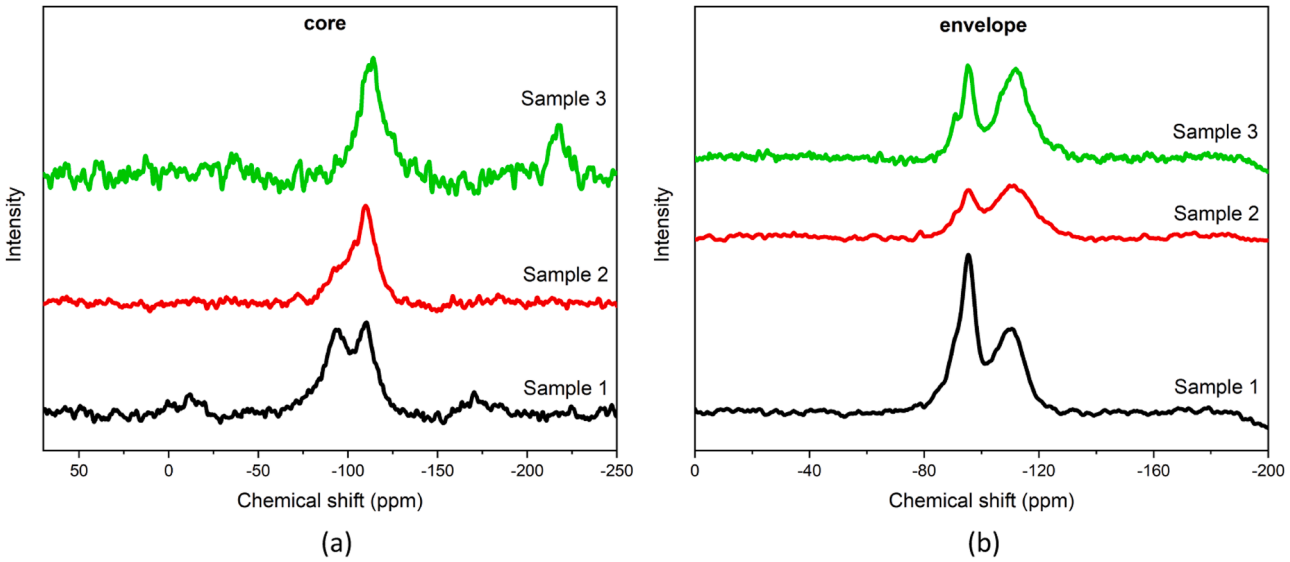

Fig. 4. ^{29}Si MAS NMR spectra of the combustion residues of the core material (a) and of the envelope (b) of Samples 1, 2, 3.

Table 2
Peak position, relative amount and assignment of the resonances in ^{29}Si MAS NMR spectra of the envelope of Sample 1 before combustion (neat) and of the combustion residues of the envelope of Samples 1, 2 and 3 (Fig. 4b).

δ ppm	Sample 1 (neat) Amount %	Sample 1 Amount %	Sample 2 Amount %	Sample 3 Amount %	Assignment
−85.9	8.2	7.2	2.8	1.8	Q^2(1Al)
−90.7	10.1	9.9	7.2	6.5	Kaolin
−95.3	30.3	31.7	12.4	21.0	Talc
−99.6	6.1	8.0	6.4	6.9	Q^3
−104.2	0.0	1.6	0.0	5.8	Q^4(1Al)
−110.1	45.3	41.5	71.3	59.6	Q^4

Table 3
Peak position, relative amount and corresponding match from ^{31}P NMR spectra of combustion residues of the core material of Samples 2 and 3 (Fig. 5a).

Sample 2 δ ppm	Amount %	Sample 3 δ ppm	Amount %	Assignment
0.5	0.3	0.5	0.1	H_3PO_4 - orthophosphate
−4.3	22.4	−10.4	16.9	$Q^{'2}$ - metal phosphonates/ end phosphate groups P-O-C - pyrophosphates
−12.6	19.4	−31.5	9.7	$Q^{'3}$ - linear polyphosphates
−31.5	27.1	−41.9	14.5	$O = P(OP/Si)_3$
−41.8	30.8	−56.9	58.8	$O = P(OP/Si^{VI})_3$

predominant in Sample 3. The proposed lineshape analysis in Table 3 highlights a complex overlapping and an attempt of attribution of the 0/−20 ppm region to $Q^{'2}$ species as metal phosphonates, pyrophosphates and end P-groups, the −20/−80 ppm region to $Q^{'2}$ species in polyphosphates (at about −30 ppm). The high-field components should be associated to phosphosilicates (at about −42 ppm and −57 ppm) in different crystalline habits [53,57]. As a matter of facts chemical shifts up to −60 and 70 ppm for cubic SiP_2O_7 have been reported [57]. In particular, Sample 3 shows a high-field shifted component at about −56 ppm that could be related to phosphate linked to 6-fold coordinate Si structures, in agreement with ^{29}Si results. In both samples, a very small amount of H_3PO_4 at about 0 ppm, as by-product, seems to be present.

Also in the case of envelopes, the ^{31}P MAS spectra (Fig. 5b) present very broad resonances, ascribable to amorphous structures. Up to 6 components can be addressed (see Table 4). The resonances show intrinsic broadness, due to the variability of both second neighbour ions and P-O-X/P-O-P bond angle and strength [46]. The small sharp peak at

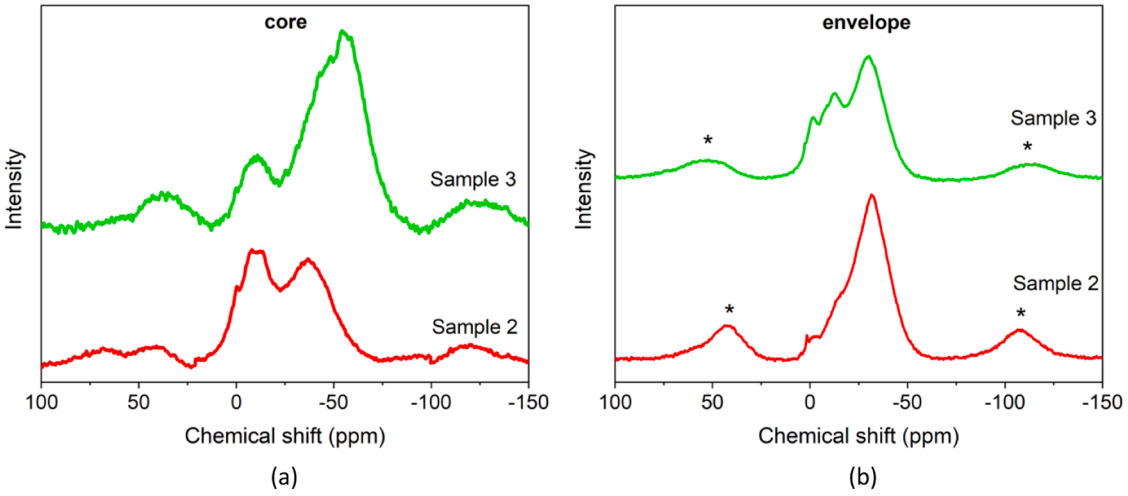

Fig. 5. ^{31}P MAS NMR spectra of the combustion residues of the core material (a) and of the envelope (b) of Samples 2 and 3. Spinning side bands are marked with *.

Table 4
Peak position, relative amount and corresponding match from ^{31}P NMR spectra of combustion residues of the envelope of Samples 2 and 3 (Fig. 5b).

Sample 2 δ ppm	Amount %	Sample 3 δ ppm	Amount %	Assignment
0.6	0.3	0.8	0.3	H_3PO_4 - orthophosphate
−1.9	1.9	−2.5	1.9	$Q^{'2}$ - metal phosphonates/
−17.5	26.2	−11.9	39.5	end phosphate groups
–	–	−14.7	1.7	P-O-C - pyrophosphates
−31.7	49.8	−31.8	47.7	$Q^{'3}$ - linear polyphosphates
−40.8	21.8	−43.1	9.0	$O = P(OP/Si)_3$

about 0 ppm indicates formation of phosphoric acid as residue due to the depolymerisation of the APP, as noticed for the cores [58]. The small broad resonance between 5 and −8 ppm could be tentatively attributed to phosphonates or end phosphate groups. The main component centred at −30 ppm is due to polyphosphates, in particular aluminium polyphosphates [44,49]. The high field shoulder at about −40 ppm could be attributed to phosphoryl group $O = P(OP/Si)_3$, where P tetrahedra are connected with Si tetrahedral, thus indicating a co-condensation of the groups [59].

3.2. X-Ray diffraction (XRD)

From the XRD diffractograms of the core material, shown in Fig. 6a, it is possible to distinguish some differences between the peaks present in Samples 1, 2 and 3. The main difference consists in the presence of silicon phosphate only in Sample 3, given by the reaction of oMMT with APP. The fact that silicon phosphate is not visible into Sample 2 means that elevated quantities of APP are required for its formation (AP423 is composed only by APP, while AP766 by APP and other synergistic components, as reported in the supplementary material). The presence of talc may be related to ablation phenomena occurring during the thermal degradation of the envelope [32,60]. The presence of cristobalite may be related to its presence in the kaolin [51,61]. From the XRD diffractograms of the envelope, shown in Fig. 6b, it is possible to observe that the three diffractograms are almost identical (only minor differences in the peak intensity can be noticed). The patterns reveals the presence of calcite, chlorite and quartz, typical contaminants of talc, present in the composition of the envelope [62]. Differently from montmorillonite, talc and quartz do not react with APP and therefore are still visible also in Samples 2 and 3. Despite the presence of talc was detected in the core and in the envelope it was not possible to detect the presence of montmorillonite.

3.3. Scanning electron microscopy (SEM)

From SEM pictures obtained in back-scattered electron (BSE) mode of the core residues of samples 1 and 2, shown in Fig. 7 (a,b), it is possible to observe the different structure of the two samples. Sample 1 seems to have a more uniform morphology, characterized by the presence of holes (due to the escape of combustion gases and paraffin degradation). Sample 2 is characterized by the presence of big holes all around the observed region, probably caused by the reaction between the multicomponent FR and the other components, mainly oMMT. Moreover, different elements can be recognised from different contrasts visible in Fig. 7b: they may be degradation products of FR in the condensed phase or the results of reactions occurred during the combustion between the FR and the different components of Sample 2.

From SEM pictures obtained in back-scattered electron (BSE) mode of the envelope material of Samples 1 and 2, shown in Fig. 8 (a-b), it is possible to observe that the two samples present similar morphologies: the surface is compact and uniform but in case of Sample 2 it contains some cracks whose origin is although difficult to clarify. On the other hand, the morphology is completely different from that of the core material with the absence of voids and porosity. Although the presence of FRs changes the morphology of the core residues, it seems clear that it does not change the morphology of the envelope residues nor the formation of two distinct intumescent layers.

3.4. Energy dispersive X-ray spectroscopy (EDX)

From the SEM images used for the EDX analysis of the combustion residues of the core material of Sample 1, shown in Fig. 9 (a,c,e), and from the corresponding results, listed in Table 5, it is possible to observe the presence of considerable quantities of silicon and aluminium. The presence of these two components may be related to the oMMT used for the shape stabilization of paraffin. Another reason for the presence of silicon and aluminium may be related to ablation phenomena occurring

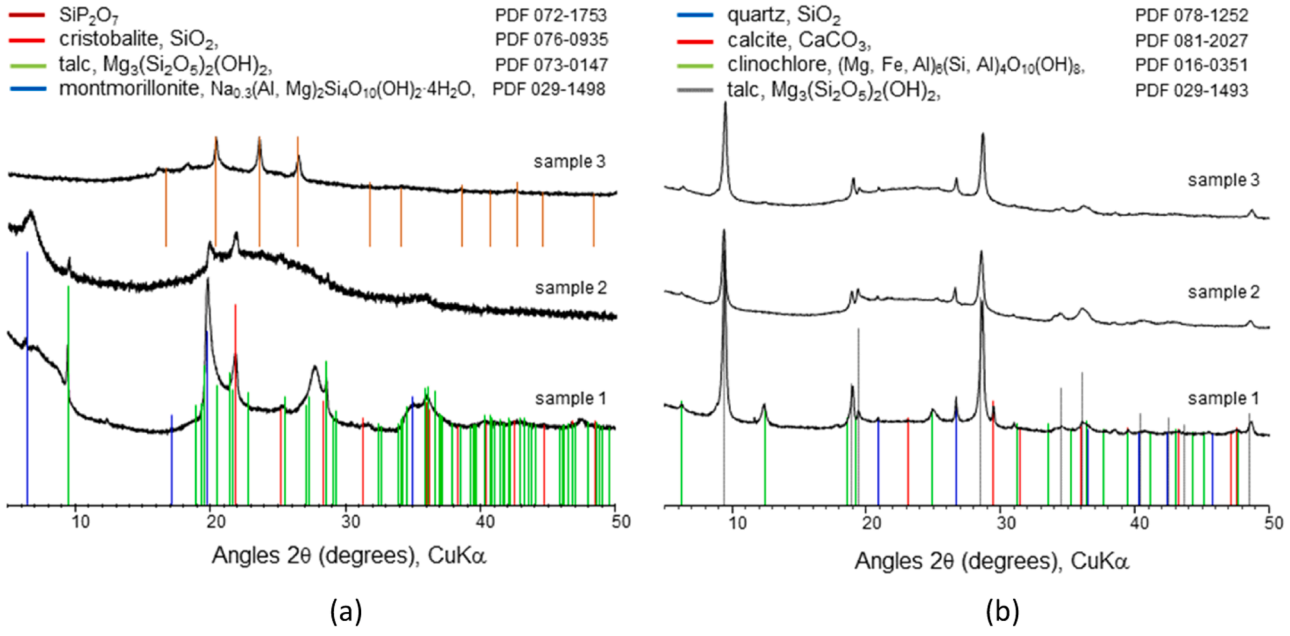

Fig. 6. XRD diffractograms of the combustion residues of Samples 1, 2 and 3: core material (a) and envelope material (b).

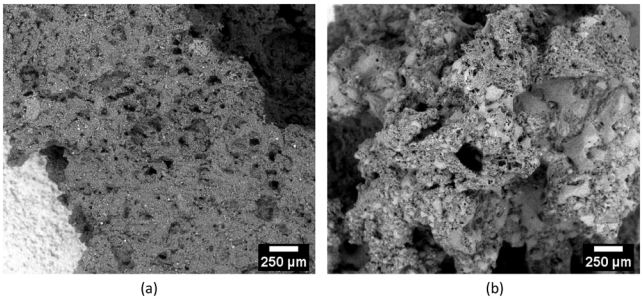

Fig. 7. SEM images at 50x of the combustion residues of the core material of Sample 1 (a) and Sample 2 (b), obtained in back-scattered electron (BSE) mode.

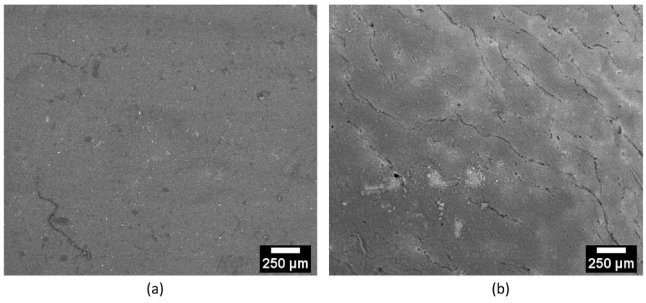

Fig. 8. SEM images at 50x of the combustion residues of the envelope material of Sample 1 (a) and Sample 2 (b), obtained in BSE mode.

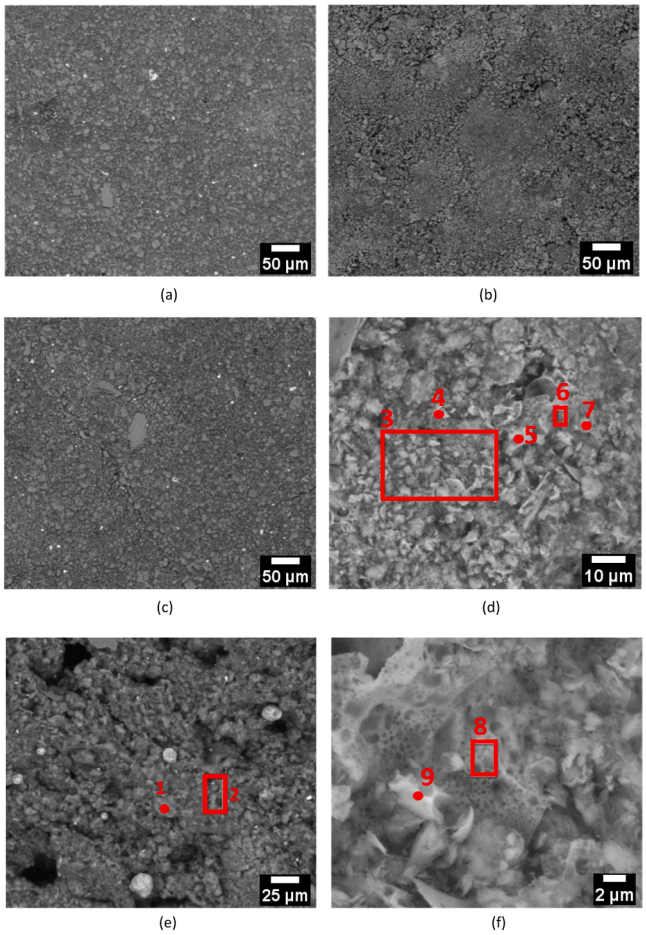

Fig. 9. SEM images used for the EDX analysis of the combustion residues of the core material of Sample 1 (a,c,e) and Sample 2 (b,d,f). EDX analyses are reported in Tables 5 and 6.

Table 5
Results of the EDX analysis of the combustion residues of the core material of Sample 1 (from Figs. 9a, 9c, 9e).

Element	Average value* [wt%]	Average value** [wt%]	spot 1 [wt%]	spot 2 [wt%]
C	44.0	43.0	28.3	40.6
O	27.6	28.3	32.5	28.5
P	–	–	–	–
Al	5.5	5.5	7.6	5.8
Si	15.3	15.6	20.6	15.7
Zn	2.4	2.7	3.4	3.1
Fe	–	–	2.9	–

* Average value referred to Fig. 9a.
** Average value referred to Fig. 9c.

during the thermal degradation of the envelope that contains kaolin, silica and talc [32,60,63]. The beneficial effect of the envelope observed in the fire characterization may be therefore related not only to the barrier effect created by the presence of talc and kaolin but also to ablation that causes a different distribution of the components making them available at the surface of the core residue.

From the SEM images used for the EDX analysis of the combustion residues of the core material of Sample 2, shown in Fig. 9 (b,d,f), and from the corresponding results, listed in Table 6, it is possible to observe the presence of considerable quantities of phosphorus and limited quantities of aluminium, silicon and zinc. The presence of phosphorus is related to the FR added to the material. The presence of aluminium and silicon may be related to the oMMT used for the shape stabilization of paraffin and to the presence of aluminium in the FR (the AP766 contains aluminium-diethyl phosphinate). The small quantities of zinc may be related to the composition of the EPDM matrix that contains ZnO. Considering the fact that AP766 is composed of 23 wt% of phosphorus (according to the TDS), and that the core of Sample 2 contains 20 wt% of FR, it is possible to evaluate the theoretical content of P within the envelope equal to 4.4 wt%. This value, normalized by the residual weight of the core material ($E + P + 766$), equal to 25.3 wt%, results to be 17.3 wt%; it seems to be not too different from the result of the EDX, around 23 wt%. These results may indicate that all the phosphorus has remained in the condensed phase. Considering the combustion mechanisms, this means that the condensed phase reactions lead to the formation of charred structure with a consequent reduced fuel production thanks to the lower amount of carbon available [24].

From the SEM images used for the EDX analysis of the combustion residues of the envelope of Sample 1, shown in Fig. 10 (a,c), and from the corresponding results, listed in Table 7, it is possible to observe the presence of considerable quantities of silicon and limited quantities of aluminium, magnesium and zinc. The presence of these elements is ascribed to the composition of the envelope that contains zinc oxide, silica, kaolin and talc.

From the SEM images used for the EDX analysis of the combustion residues of the envelope of Sample 2, shown in Fig. 10 (b,d), and from the corresponding results, listed in Table 8, it is possible to observe the presence of limited quantities of phosphorus and silicon. The presence of silicon is probably related to the composition of the envelope that contains silica, kaolin and talc. The small quantities of aluminium detected in spectra 13 and 15 (see Table 8) may be related to the FR (the AP766 contains aluminium diethyl phosphinate). Considering the fact that AP766 is composed of 23 wt% of phosphorus (according to the TDS), and that the core of Sample 2 contains 18 wt% of FR, it is possible to evaluate the theoretical content of P within the envelope equal to 4.1 wt%. This value, normalized by the residual weight of the envelope (ENV+766), equal to 60.8 wt%, results to be 6.8 wt%, close to the result of the EDX, around 8 wt%. These results may indicate that, similarly to the core material, all the phosphorus has remained in the condensed phase.

Table 6
Results of the EDX analysis of the combustion residues of the core material of Sample 2 (from Figs. 9b, 9d, 9f).

Element	Average value* [wt%]	spot 3 [wt%]	spot 4 [wt%]	spot 5 [wt%]	spot 6 [wt%]	spot 7 [wt%]	spot 8 [wt%]	spot 9 [wt%]
C	32	32	27	27	28	25	26	24
O	34	37	41	27	37	29	27	32
P	18	14	19	30	18	28	30	27
Al	4	4	3	5	4	5	5	5
Si	–	8	5	7	7	7	5	–
Zn	–	8	5	7	7	7	5	–

* Average value referred to Fig. 9b.

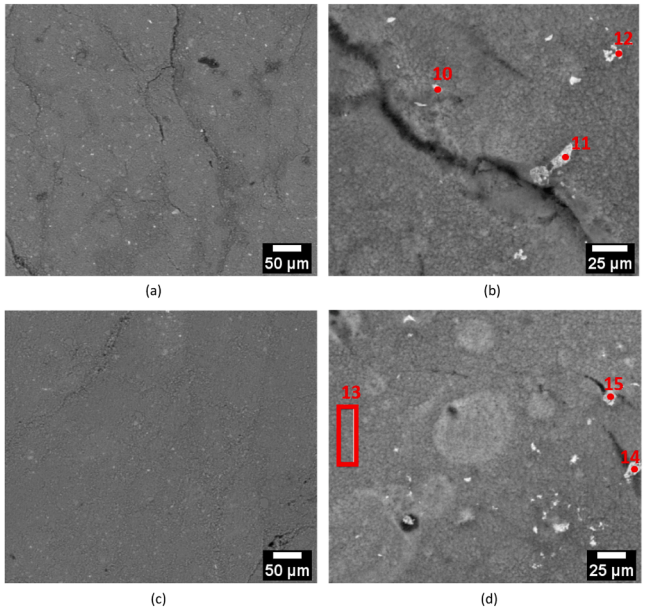

Fig. 10. SEM images used for the EDX analysis of the combustion residues of the envelope of Sample 1 (a,c) and Sample 2 (b,d). EDX analyses are reported in Tables 7 and 8.

Table 7
Results of the EDX analysis of the combustion residues of the envelope of Sample 1.

Element	Average value* [wt%]	Average value** [wt%]
C	14.1	12.6
O	42.6	43.8
P	–	–
Al	4.2	4.3
Si	24.0	24.7
Zn	4.0	2.8
Mg	7.1	7.5
Mo	2.5	2.2

* Average value referred to Fig. 10a.
** Average value referred to Fig. 10c.

4. Conclusions

In this work the combustion residues obtained from cone calorimeter tests performed on EPDM/NBR panels containing paraffin for thermal energy storage applications, whose fire behaviour had been improved using two FRs based on ammonium polyphosphate, were investigated and compared in order to better evaluate the mechanism of flame reaction. The multinuclear NMR study of both core and envelope highlighted the different routes of structural evolution characterized by the formation of char and structural rearrangements of the inorganic components. In particular, it was observed the great reactivity of montmorillonite in presence of phosphates, the formation of different Al-O-P compounds (due to the presence of aluminium diethylphosphinate in the composition of AP766) and of Si-O-P compounds (due to the presence of talc and kaolin in the envelope). From XRD analysis it was verified the formation of silicon phosphate from the reaction of ammonium polyphosphate with the montmorillonite, while using the AP423 as FR due to the higher phosphorus content with respect to AP766. The observed interactions can explain the beneficial effect related to the presence of montmorillonite and of the envelope and the best performances of fire retardant AP766 observed in the first part of this work [37]. From SEM images it was possible to observe the different morphology of samples with and without FR: samples with FR were characterized by the presence of holes probably caused by the degradation of FR, while samples without FR by a more homogeneous structure. From EDX analyses it was possible to detect the presence of phosphorus in quantities comparable to the initial ones, indicating the possibility that all the phosphorus remained in the condensed phase during the combustion. Consequently, the mechanism of fire behaviour seemed to occur essentially in the condensed phase with the formation of a charred structure that reduced the fuel production thanks to the lower amount of carbon available.

Table 8
Results of the EDX analysis of the combustion residues of the envelope of Sample 2 (from Figs. 10b, 10d).

Element	spot 10 [wt%]	spot 11 [wt%]	spot 12 [wt%]	spot 13 [wt%]	spot 14 [wt%]	spot 15 [wt%]
C	56.4	56.7	58.9	65.0	52.7	49.1
O	26.0	24.4	24.4	13.1	28.0	31.5
P	6.3	9.3	6.6	8.6	9.1	8.1
Al	–	–	–	2.2	–	2.4
Si	5.7	4.0	5.2	7.9	4.9	6.5
Zn	–	2.1	–	–	–	–

CRediT authorship contribution statement

Francesco Valentini: Conceptualization, Data curation, Formal analysis, Investigation, Methodology, Validation, Visualization, Writing – original draft. **Emanuela Callone:** Formal analysis, Investigation, Methodology, Validation, Writing – original draft. **Sandra Dirè:** Formal analysis, Methodology, Validation, Writing – review & editing. **Jean-Claude Roux:** Investigation, Methodology, Validation. **Josè-Marie Lopez-Cuesta:** Conceptualization, Formal analysis, Methodology, Validation, Writing – review & editing. **Gwenn le-Saout:** Formal analysis, Investigation, Methodology, Validation. **Luca Fambri:** Methodology, Validation, Supervision, Writing – review & editing. **Andrea Dorigato:** Supervision, Writing – review & editing. **Alessandro Pegoretti:** Methodology, Supervision, Funding acquisition, Writing – review & editing.

Declaration of Competing Interest

The authors declare that they have no known competing financial interests or personal relationships that could have appeared to influence the work reported in this paper.

Data availability

Data will be made available on request.

Acknowledgements

This work was partially funded by Provincia Autonoma di Trento (Italy) through Legge 6/99, project “Compositi elastomerici a transizione di fase [E-PCM] prat. n. 23–16″.

Supplementary materials

Supplementary material associated with this article can be found, in the online version, at doi:10.1016/j.polymdegradstab.2023.110470.

References

[1] J. Xu, R.Z. Wang, Y. Li, A review of available technologies for seasonal thermal energy storage, Solar Energy 103 (2014) 610–638.
[2] Intergovernmental Panel on Climate Change. Climate Change 2014: mitigation of Climate Change. Working Group III Contribution to the IPCC Fifth Assessment Report. 2015.
[3] A. GhaffarianHoseini, N.D. Dahlan, U. Berardi, A. GhaffarianHoseini, N. Makaremi, M. GhaffarianHoseini, Sustainable energy performances of green buildings: a review of current theories, implementations and challenges, Renew. Sustain. Energy Rev. 25 (2013) 1–17.
[4] G. Li, X. Zheng, Thermal energy storage system integration forms for a sustainable future, Renew. Sustain. Energy Rev. 62 (2016) 736–757.
[5] S. Ould Amrouche, D. Rekioua, T. Rekioua, S. Bacha, Overview of energy storage in renewable energy systems, Int. J. Hydrogen Energy 41 (45) (2016) 20914–20927.
[6] Eurostat. Energy consumption and use by households. 2020; Available from: https://ec.europa.eu/eurostat/web/products-eurostat-news/-/DDN-20200626-1#:~:text=Energy%20consumption%20in%20households%20by%20type%20of%20end%2Duse&text=Main%20cooking%20devices%20require%206.1,final%20energy%20consumed%20by%20households.
[7] K. Kaygusuz, The Viability of Thermal Energy Storage, Energy Sources 21 (8) (1999) 745–755.
[8] H. Bo, E.M. Gustafsson, F. Setterwall, Phase transition temperature ranges and storage density of paraffin wax phase change materials, Energy 24 (12) (1999) 1015–1028.
[9] B. He, V. Martin, F. Setterwall, Phase transition temperature ranges and storage density of paraffin wax phase change materials, Energy 29 (11) (2004) 1785–1804.
[10] S. Peng, A. Fuchs, R.A. Wirtz, Polymeric phase change composites for thermal energy storage, J. Appl. Polym. Sci. 93 (2004) 1240–1251.
[11] A.M. Borreguero, M. Carmona, M.L. Sanchez, J.L. Valverde, J.F. Rodriguez, Improvement of the thermal behaviour of gypsum blocks by the incorporation of microcapsules containing PCMS obtained by suspension polymerization with an optimal core/coating mass ratio, Appl. Therm. Eng. 30 (10) (2010) 1164–1169.
[12] A. Dorigato, M.V. Ciampolillo, A. Cataldi, M. Bersani, A. Pegoretti, Polyethylene wax/EPDM blends as shape-stabilized phase change materials for thermal energy storage, Rubber Chem. Technol. 90 (3) (2017) 575–584.
[13] F. Valentini, L. Fambri, A. Dorigato, A. Pegoretti, Production and Characterization of TES-EPDM Foams With Paraffin for Thermal Management Applications, Front. Mater. 8 (2021) 101.
[14] H. Bo, E.M. Gustafsson, F. Setterwall, Tetradecane and hexadecane binary mixtures as phase change materials (PCMs) for cool storage in district cooling systems, Energy 24 (12) (1999) 1015–1028.
[15] Á.Á. Pardiñas, M.J. Alonso, R. Diz, K.H. Kvalsvik, J. Fernández-Seara, State-of-the-art for the use of phase-change materials in tanks coupled with heat pumps, Energy Build. 140 (2017) 28–41.
[16] A. Shukla, D. Buddhi, R.L. Sawhney, Solar water heaters with phase change material thermal energy storage medium: a review, Renew. Sustain. Energy Rev. 13 (8) (2009) 2119–2125.
[17] M.A. Fazilati, A.A. Alemrajabi, Phase change material for enhancing solar water heater, an experimental approach, Energy Convers. Manag. 71 (2013) 138–145.
[18] A. Kürklü, A. Özmerzi, S. Bilgin, Thermal performance of a water-phase change material solar collector, Renew. Energy 26 (3) (2002) 391–399.
[19] A. Kasaeian, L. Bahrami, F. Pourfayaz, E. Khodabandeh, W.-M. Yan, Experimental studies on the applications of PCMs and nano-PCMs in buildings: a critical review, Energy Build. 154 (2017) 96–112.
[20] X. Kong, C. Yao, P. Jie, Y. Liu, C. Qi, X. Rong, Development and thermal performance of an expanded perlite-based phase change material wallboard for passive cooling in building, Energy Build. 152 (2017) 547–557.
[21] C. Yao, X. Kong, Y. Li, Y. Du, C. Qi, Numerical and experimental research of cold storage for a novel expanded perlite-based shape-stabilized phase change material wallboard used in building, Energy Convers. Manag. 155 (2018) 20–31.
[22] L.F. Cabeza, C. Castellón, M. Nogués, M. Medrano, R. Leppers, O. Zubillaga, Use of microencapsulated PCM in concrete walls for energy savings, Energy Build. 39 (2) (2007) 113–119.
[23] F. Valentini, A. Dorigato, L. Fambri, M. Bersani, M. Grigiante, A. Pegoretti, Production and characterization of novel EPDM/NBR panels with paraffin for potential thermal energy storage applications, Therm. Sci. Eng. Progr. (2022) 32.
[24] P. Sittisart, M.M. Farid, Fire Retardant for Phase Change Material, Flame Retardants (2015) 187–207.
[25] Y. Cai, Y. Hu, L. Song, Y. Tang, R. Yang, Y. Zhang, Z. Chen, W. Fan, Flammability and thermal properties of high density polyethylene/paraffin hybrid as a form-stable phase change material, J. Appl. Polym. Sci. 99 (4) (2006) 1320–1327.
[26] R. Kozlowski, D. Wesolek, M. Wladyka-Przybylak, S. Duquesne, A. Vannier, S. Bourbigot, R. Delobel, Intumescent Flame-Retardant Treatments for Flexible Barriers. Multifunctional Barriers for Flexible Structure. Materials Science, Springer, Berlin, Heidelberg: Berlin, 2007.
[27] Y. Cai, Y. Hu, L. Song, Q. Kong, R. Yang, Y. Zhang, Z. Chen, W. Fan, Preparation and flammability of high density polyethylene/paraffin/organophilic montmorillonite hybrids as a form stable phase change material, Energy Convers. Manag. 48 (2) (2007) 462–469.
[28] F. Dabrowski, M. Le Bras, L. Cartier, S. Bourbigot, The Use of Clay in an EVA-Based Intumescent Formulation. Comparison with the Intumescent Formulation Using Polyamide-6 Clay Nanocomposite As Carbonisation Agent, J. Fire Sci. 19 (3) (2016) 219–241.
[29] S.-H. Chiu, W.-K. Wang, Dynamic flame retardancy of polypropylene filled with ammonium polyphosphate, pentaerythritol and melamine additives, Polymer (Guildf) 39 (10) (1998) 1951–1955.
[30] Y. Tang, Y. Hu, S. Wang, Z. Gui, Z. Chen, W. Fan, Intumescent flame retardant-montmorillonite synergism in polypropylene-layered silicate nanocomposites, Polym. Int. 52 (8) (2003) 1396–1400.
[31] Y. Cai, Y. Hu, L. Song, H. Lu, Z. Chen, W. Fan, Preparation and characterizations of HDPE–EVA alloy/OMT nanocomposites/paraffin compounds as a shape stabilized phase change thermal energy storage material, Thermochim. Acta 451 (1–2) (2006) 44–51.
[32] M. Zanetti, T. Kashiwagi, L. Falqui, G. Camino, Cone Calorimeter Combustion and Gasification Studies of Polymer Layered Silicate Nanocomposites, Chem. Mater. 14 (2) (2002) 881–887.
[33] Y.B. Cai, Q.F. Wei, D.F. Shao, Y. Hu, L. Song, W.D. Gao, Magnesium hydroxide and microencapsulated red phosphorus synergistic flame retardant form stable phase change materials based on HDPE/EVA/OMT nanocomposites/paraffin compounds, J. Energy Inst. 82 (1) (2009) 28–36.
[34] X. Almeras, M.L. Bras, P. Hornsby, S. Bourbigot, G. Marosi, S. Keszei, F. Poutch, Effect of fillers on the fire retardancy of intumescent polypropylene compounds, Polym. Degrad. Stab. 82 (2) (2003) 325–331.
[35] H.H. Dzulkafli, F. Ahmad, S. Ullah, P. Hussain, O. Mamat, P.S.M. Megat-Yusoff, Effects of talc on fire retarding, thermal degradation and water resistance of intumescent coating, Appl. Clay Sci. 146 (2017) 350–361.
[36] T. Thuechart, W. Keawwattana, The Effect of Kaolin Clay on Fire Retardancy and Thermal Degradation of Intumescent Flame Retardant (IFR)/Natural Rubber Composite, Adv. Mat. Res. 844 (2013) 334–337.
[37] F. Valentini, J.-C. Roux, J.-M. Lopez-Cuesta, L. Fambri, A. Dorigato, A. Pegoretti, Fire behaviour of EPDM/NBR panels with paraffin for thermal energy storage applications. Part 1: fire behaviour, Polym. Degrad. Stab. 207 (2023), 110240.
[38] P. Hough, N. van der Aar, Z. Qiu, Compounding and Mixing Methodology for Good Performance of EPDM in Tire Sidewalls, Tire Sci. Technol. 48 (1) (2020) 2–21.
[39] A. Nasiri, N. Gontard, E. Gastaldi, S. Peyron, Contribution of nanoclay to the additive partitioning in polymers, Appl. Clay Sci. 146 (2017) 27–34.
[40] J.E. Jablonski, L. Yu, S. Malik, A. Sharma, A. Bajaj, S.L. Balasubramaniam, R. Bleher, R.G. Weiner, T.V. Duncan, Migration of Quaternary Ammonium Cations from Exfoliated Clay/Low-Density Polyethylene Nanocomposites into Food Simulants, ACS Omega 4 (8) (2019) 13349–13359.
[41] A.A. Mousa, Y.A. Youssef, W.S. Mohamed, R. Farouk, E. Giebel, M.R. Buchmeiser, Organoclays assisted vat and disperse dyeing of poly(ethylene terephthalate) nanocomposite fabrics via melt spinning, Coloration Technol. 134 (2) (2017) 126–134.
[42] J.-B. d’Espinose de Lacaillerie, C. Fretigny, D. Massiot, MAS NMR spectra of quadrupolar nuclei in disordered solids: the Czjzek model, J. Magn. Reson. 192 (2) (2008) 244–251.
[43] D. Massiot, F. Fayon, M. Capron, I. King, S.L. Calvé, B. Alonso, J.-O. Durand, B. Bujoli, Z. Gan, G. Hoatson, Modelling one- and two-dimensional solid-state NMR spectra, Magn. Reson. Chem. 40 (1) (2002) 70–76.
[44] A.D. Naik, G. Fontaine, F. Samyn, X. Delva, J. Louisy, S. Bellayer, Y. Bourgeois, S. Bourbigot, Mapping the multimodal action of melamine-poly(aluminium phosphate) in the flame retardancy of polyamide 66, RSC Adv. 4 (35) (2014) 18406–18418.
[45] F. Samyn, S. Bourbigot, Thermal decomposition of flame retarded formulations PA6/aluminum phosphinate/melamine polyphosphate/organomodified clay: interactions between the constituents? Polym. Degrad. Stab. 97 (11) (2012) 2217–2230.
[46] S. Bourbigot, M. Le Bras, R. Delobel, Carbonization mechanisms resulting from intumescence association with the ammonium polyphosphate-pentaerythritol fire retardant system, Carbon N Y 31 (8) (1993) 1219–1230.
[47] E. Callone, R. Ceccato, F. Deflorian, M. Fedel, S. Dirè, Filler-matrix interaction in sodium montmorillonite-organosilica nanocomposite coatings for corrosion protection, Appl. Clay Sci. 150 (2017) 81–88.
[48] M. Fedel, E. Callone, S. Diré, F. Deflorian, M.G. Olivier, M. Poelman, Effect of Na-Montmorillonite sonication on the protective properties of hybrid silica coatings, Electrochim. Acta 124 (2014) 90–99.

[49] S. Bellayer, M. Jimenez, B. Prieur, B. Dewailly, A. Ramgobin, J. Sarazin, B. Revel, G. Tricot, S. Bourbigot, Fire retardant sol-gel coated polyurethane foam: mechanism of action, Polym. Degrad. Stab. 147 (2018) 159–167.
[50] S. Duquesne, G. Fontaine, O. Céerin-Delaval, B. Gardelle, G. Tricot, S. Bourbigot, Study of the thermal degradation of an aluminium phosphinate-aluminium trihydrate combination, Thermochim. Acta 551 (2013) 175–183.
[51] J. Rocha, J. Klinowski, 29Si and 27Al Magic-angle-spinning NMR Studies of the Thermal Transformation of Kaolinite, Phys. Chem. Miner. 17 (1990) 179–186.
[52] L. Martel, A. Kovacs, K. Popa, D. Bregiroux, T. Charpentier, (31)P MAS NMR and DFT study of crystalline phosphate matrices, Solid State Nucl. Magn. Reson. 105 (2020), 101638.
[53] C. Lejeune, C. Coelho, L. Bonhomme-Coury, T. Azaïs, J. Maquet, C. Bonhomme, Studies of silicophosphate derivatives by 31P→29Si CP MAS NMR, Solid State Nucl. Magn. Reson. 27 (4) (2005) 242–246.
[54] S. Mostoni, M. D'Arienzo, B. Di Credico, L. Armelao, M. Rancan, S. Dire, E. Callone, R. Donetti, A. Susanna, R. Scotti, Design of a Zn Single-Site Curing Activator for a More Sustainable Sulfur Cross-Link Formation in Rubber, Ind. Eng. Chem. Res. 60 (28) (2021) 10180–10192.
[55] C.A.R. Reyes, C. Williams, O.M.C. Alarcón, Nucleation and growth process of sodalite and cancrinite from kaolinite-rich clay under low-temperature hydrothermal conditions, Mater. Res. 16 (2) (2013) 424–438.
[56] K.J.D. MacKenzie, R.H. Meinhold, The thermal reactions of talc studied by 29Si and 25 Mg MAS NMR, Thermochim. Acta 244 (1994) 195–203.
[57] C. Coelho, T. Azais, L. Bonhomme-Coury, J. Maquet, D. Massiot, C. Bonhomme, Application of the MAS-J-HMQC experiment to a new pair of nuclei {29Si,31P}: si5O(PO4)6 and SiP2O7 polymorphs, J. Magn. Reson. 179 (1) (2006) 114–119.
[58] Yang, C.Q., Flame Resistant cotton, in Handbook of Fire Resistant Textiles, F.S. Kilinc, Editor. 2013, Woodhead Publishing. p. 177–220.
[59] N.J. Clayden, S. Esposito, P. Pernice, A. Aronne, Solid state 29Si and 31P NMR study of gel derived phosphosilicate glasses, J. Mater. Chem. 11 (3) (2001) 936–943.
[60] B. Fiorentino, R. Fulchiron, V. Bounor-Legaré, J.-C. Majesté, J.C. Leblond, J. Duchet-Rumeau, Chemical modification routes of synthetic talc: influence on its nucleating power and on its dispersion state, Appl. Clay Sci. 109-110 (2015) 107–118.
[61] H.M. Zhou, X.C. Qiao, J.G. Yu, Influences of quartz and muscovite on the formation of mullite from kaolinite, Appl. Clay Sci. 80-81 (2013) 176–181.
[62] Imerys S.A. Technical datasheet of Mistron® R10 C. Visited on 29/09/2021; Available from: https://materials.ulprospector.com/en/profile/odm?tds&docid=234166.
[63] A.R. Bahramian, M. Kokabi, M.H.N. Famili, M.H. Beheshty, Ablation and thermal degradation behaviour of a composite based on resol type phenolic resin: process modeling and experimental, Polymer (Guildf) 47 (10) (2006) 3661–3673.